ELSEVIER

Journal of Non-Crystalline Solids 263&264 (2000) 251–262

JOURNAL OF NON-CRYSTALLINE SOLIDS

www.elsevier.com/locate/jnoncrysol

Optical loss and Nd^{3+} non-radiative relaxation by Cu, Fe and several rare earth impurities in phosphate laser glasses

P.R. Ehrmann [a,*], J.H. Campbell [a], T.I. Suratwala [a], J.S. Hayden [b], D. Krashkevich [b], K. Takeuchi [c]

[a] *Lawrence Livermore National Laboratory, P.O. Box 808, L-500, Livermore, CA 94550, USA*
[b] *Schott Glass Technologies, Inc., 400 York Ave., Duryea, PA 18642, USA*
[c] *Hoya Corporation, USA, 3400 Edison Way, Fremont, CA 94538, USA*

Abstract

Extinction coefficients (at 1053 nm) and Nd^{3+} fluorescence quenching rates are reported for Cu, Fe, Dy, Pr, Sm and Ce at doping concentrations up to 1000 ppmw in two meta-phosphate laser glasses melted under oxidizing conditions (1 atmosphere O_2). The extinction coefficient and quenching rate for Cu are $2.7(\pm 0.1) \times 10^{-3}$ cm^{-1}/ppmw and 10.4 ± 0.2 Hz/ppmw, respectively. The extinction coefficient and quenching rate for Fe are concentration dependent below 300 ppmw due to an observed change in Fe^{2+}/Fe^{3+} distribution; an empirically derived expression is used to describe this effect. The extinction coefficient and quenching rates for Dy, Pr and Sm, are nearly the same: 1.6, 1.2 and $1.3(\pm 0.05) \times 10^{-5}$ cm^{-1}/ppmw and 0.89, 0.72 and 0.63 ± 0.04 Hz/ppmw, respectively, while those for Ce are less: $0.84(\pm 0.03) \times 10^{-5}$ cm^{-1}/ppmw and 0.061 ± 0.03 Hz/ppmw. The quenching results are explained using the Förster–Dexter theory for dipolar energy transfer.

1. Introduction

Neodymium-doped phosphate glasses are the preferred material for use in high-energy and high-peak-power laser systems [1–3]. There are a number of reasons for this choice, but perhaps the three most important are: (1) energy can be efficiently stored and extracted from these glasses [4,5], (2) high energy storage densities ($\geqslant 250$ J/l) can be achieved [2,4] and (3) the glasses can be manufactured in meter-scale sizes with high optical homogeneity and low Pt-inclusion concentrations [6].

Transition metal and rare earth ion impurities degrade the laser performance of the glass by reducing both the stored energy and optical transmission [7]. The stored energy, which refers to the Nd^{3+} excited state density in the $^4F_{3/2}$ upper laser level, is affected by these impurities through increased non-radiative losses. In addition, the optical absorption of many transition metal impurities contributes to absorption losses at the laser wavelength, even at contaminant concentrations in the low ppmw range. In this regard, Fe and Cu are particularly troublesome: Fe because it is present in most materials due to the use of iron-based processing equipment and Cu because of its exceptionally large optical absorption cross-section at the 1053 nm laser transition. For these reasons, Fe and Cu are the main focus of this study. We also examine Dy, Pr, Sm and Ce

* Corresponding author. Tel.: +1-925 423 2949; fax: +1-925 423 0792.
E-mail address: chrmann1@llnl.gov (P.R. Ehrmann).

0022-3093/00/$ - see front matter
PII: S0022-3093(99)00682-1

contaminants because they are difficult elements to separate from Nd and therefore are common impurity ions in Nd raw materials [6].

Optical absorption by impurities decreases the net gain of a laser glass amplifier. For example, in the small-signal region, the amplifier gain, G_{SS}, is

$$G_{SS} = \frac{F_{out}}{F_{in}} = \exp((g_0 - \alpha)l), \quad (1)$$

where F_{in} and F_{out} are the input and output fluence (J/cm^2), respectively, l, the laser glass length (cm), and g_0 the gain coefficient (cm^{-1}) [5]. Here α represents the sum of all optical loss terms

$$\alpha = \alpha_{scatter} + \sum_{i=1}^{n} \alpha_{TM_i} + \sum_{j=1}^{n} \alpha_{RE_j}, \quad (2)$$

where $\alpha_{scatter}$ is the loss coefficient (cm^{-1}) due to scattering by defects and inclusions (such as bubbles and Pt particles), and α_{TM_i} and α_{RE_j} represent the individual absorption coefficients due to transition metal ion, i, and rare earth ion, j, respectively. The absorption coefficient for a given ion is the product of the extinction coefficient, ε (cm^{-1}/ppmw) and the impurity concentration, c (ppmw). Generally, scatter losses are negligible (in the absence of laser damage) because of the highly polished surfaces and the lack of inclusions or bubbles in the laser glasses used on laser systems [8]. Therefore, absorption by impurities is the dominant loss term.

Apart from increasing the optical losses, (α), impurities can also adversely effect laser performance by decreasing the stored energy through non-radiative energy losses [4,7]. The rate of energy transfer between Nd^{3+} and an impurity is generally described on the basis of a dipole–dipole interaction using the model originally formulated by Förster [9] and later extended by Dexter [10]. In the Förster–Dexter model, Nd^{3+} is the 'donor' (D) and the impurity the 'acceptor' (A); the energy transfer rate is given as

$$k_{DA} = \eta R_{DA}^{-6} \int \frac{G_D(v) K_A(v)\, dv}{v^4}, \quad (3)$$

where η is a constant for a given base glass composition and R_{DA} is the inter-atomic distance between the donor and acceptor. The integral describes the spectral overlap between the donor emission, $G_D(v)$ and acceptor absorption $K_A(v)$, where v is in wave numbers. Thus acceptors that are the strongest absorbers at the emission wavelength tend to produce the greatest increase in the non-radiative decay rate.

There have been numerous studies of the optical absorption properties of Fe and other transition metal ions in phosphate glasses (see for example [11–22]) and fluorophosphate glasses [20,21,23–26]. However, only a few previous studies have addressed the issue of optical loss at 1053 nm and/or fluorescence quenching by transition metal and rare earth ions present at impurity levels of $\lesssim$1000 ppmw in Nd-doped phosphate laser glasses [7,27–29]. In this work, we report for the first time both the absorption loss and the increase in Nd^{3+} non-radiative decay rate due to Fe and Cu over a range of doping concentrations from about 10 to 1000 ppmw in two widely used commercial meta-phosphate glasses: LHG-8 and LG-770. We also report the absorption loss and fluorescence quenching by several common rare earth impurities (Dy, Pr, Sm and Ce) doped mostly at 1000 ppmw. All melting has been carried out in an oxidizing environment (O_2 gas; 1 atm) because these conditions are widely used in commercial laser glass processing [6,30,31].

2. Experimental

2.1. Preparation and chemical analysis of glass melts

The two glass compositions used in this study are LHG-8 and LG-770. LHG-8 has the composition (mol%): (55–60)P_2O_5–(8–12)Al_2O_3–(13–17)K_2O–(10–15)BaO and (0–2)Nd_2O_3; similarly LG-770 is (58–62)P_2O_5–(6–10)Al_2O_3–(20–25)K_2O–(5–10)MgO and (0–2)Nd_2O_3. Both glasses are near meta-phosphates (O/P $\sim$ 3.0). The compositions are reported as ranges to account for variability due to doping and melting methods and to protect certain proprietary aspects of the compositions [4,6]. Several recent studies have shown that the

laser, optical, and physical properties of these two glasses are quite similar (±10% for most properties) suggesting that over the minor ranges in composition (and modifiers) listed above, the laser glass properties are largely unchanged [4,6,32].

All glasses were prepared using procedures described elsewhere [27,29] and using the same source and purity starting materials. Impurity concentrations were verified by chemical analysis as described below. Several undoped samples were prepared as references. All samples were melted in quartz crucibles with both dry O_2 bubbling and dry O_2 cover gas and homogenized by stirring; prior to melting both the crucible and stirrer were cleaned with 6 M HCl to minimize contamination. The LG-770 samples were first melted at 1200°C and then refined for four hours at 1375°C to remove bubbles. The LHG-8 samples were prepared in a similar fashion using melt temperatures of 1100°C and refining at 1250°C. In the case of both LHG-8 and LG-770, the liquid was then cooled to approximately 900°C and cast into a mold. The samples were then annealed to reduce residual stress at a rate of about 30°C/h starting at approximately 500°C (~50°C above T_g) and ending near room temperature.

The use of a dry cover gas during melting was to minimize hydroxyl group contamination caused by water vapor reacting with the glass [6,33]. The OH concentration was measured by the intensity of the O–H vibration band near 3000 cm^{-1} [34,35]. The measured absorption at 3000 cm^{-1} for the LG-770 samples was $\lesssim 0.6\ cm^{-1}$ and for the LHG-8 samples $\lesssim 5\ cm^{-1}$.

The impurity doping concentration of each sample was verified by analysis of fully dissolved glass solutions using inductively coupled plasma (ICP) emission spectrometry (Thermo Iris Model 6943) for Fe and Cu and ICP mass spectrometry (Hewlett Packard Model 4500) for the rare earths. Sc, Be and/or Pr were used as internal standards depending on the analyte. National Institute of Standards and Technology traceable standards (SPEX Industries) were used to calibrate the instruments. The measured dopant ion concentrations in the glasses were in close agreement with the batch compositions (±10%).

2.2. Nd^{3+} fluorescence decay

The fluorescence decay rates were measured using $2\times2\times2$ mm^3 polished glass cubes. The sample was held in an anodized mount and illuminated with the broadband spectral output (~300–1100 nm) from a flashlamp (EG&G LS1130-4) having a 2.2 μs pulse-width. Two optical filters (Melles Griot KG-3 and BG-18) effectively blocked all but the visible pump wavelengths (340–620 nm). A photo-multiplier tube (Hamamatsu R5108), mounted perpendicular to the flashlamp, monitored the fluorescence signal. An optical filter on the photo-multiplier (Melles Griot RG-850) blocked the pump light and allowed transmission of the fluorescence signal. The temporal decay of the signal was recorded on an oscilloscope (Tektronix TDS 380) and fit to a single exponential function to determine the characteristic Nd^{3+} fluorescence decay time. A signal generator (Tucker Electronics, TFG 8140) is used to trigger the flashlamp and oscilloscope. The fluorescence lifetimes were corrected for non-radiative decay due to OH contamination using the empirical correlation developed by Campbell and Suratwala [4]. Also, a minor correction was made ($\leqslant 20$ Hz) for radiation trapping within the finite sample volume [36].

2.3. Optical absorption measurements

Optical extinction coefficients were measured using both a conventional spectrophotometer and a custom-built laser calorimeter. The calorimeter method was used to confirm the spectrophotometric measurements on glasses doped with Fe concentrations. Calorimetric measurements were performed at 1064 nm using a steady-state laser heating technique; details of this method are described elsewhere [8,37].

Transmission measurements were carried out with a spectrophotometer (Shimadzu model UV-1601 PC) using two polished samples of the same glass but with different thickness (5 and 50 mm) to compensate for fresnel surface losses. A series of four transmission measurements per sample were made to eliminate effects by striae or inclusions; for these measurements the samples were rotated

about the beam axis within the spectrophotometer. The average of the four transmission measurements was used to compute the absorption coefficient (α, cm^{-1}) using the exponential form of Beer's law [38]. The extinction coefficient (ε, cm^{-1}/ppmw) was then computed from the absorption coefficient and the doping concentration (c, ppmw); $\varepsilon = \alpha/c$.

The optical absorption measurements at 1053 nm were corrected for absorption by Nd^{3+} ions that thermally populate the $^4I_{11/2}$ terminal laser level using the empirical expression [4]

$$\alpha_{Nd}(T) = 1.03 \times 10^{-20}\ [Nd^{3+}]\ \exp\left(\frac{-2576}{T}\right), \quad (4)$$

where $\alpha_{Nd}(T)$ is the loss (cm^{-1}), $[Nd^{3+}]$ the Nd-dopant ion concentration (ions/cm^3) and T the temperature (K). The Nd^{3+} concentrations used in this study are 4.6×10^{20} and 4.2×10^{20} ions/cm^3 for the LG-770 and LHG-8 samples, respectively. Therefore the corresponding 1054-nm absorptions at 22°C (295 K) due to the Nd^{3+} are 7.6×10^{-4} and 7.0×10^{-4} cm^{-1}, respectively.

No attempt was made to correct for scatter losses in these optical quality glasses because the surfaces were highly polished and prepared using the same polishing procedure. Accurate measurements of scatter losses on highly polished pieces of phosphate laser glasses have been reported previously using an integrating sphere scatterometer [8]; the results show surface losses of less than 5×10^{-5} per surface and bulk glasses losses $<10^{-5}$ cm^{-1} (detection limit).

3. Results

3.1. Optical measurements

The measured optical transmission spectra between 800 and 1100 nm for Nd-doped LG-770 containing various concentrations of Fe and Cu are shown in Fig. 1. The absorption bands at about 815 and 870 nm are due to the Nd^{3+} transitions from the $^4I_{9/2}$ ground state to the overlying $^4F_{3/2}$ and $^4F_{5/2}$, $^2H_{9/2}$ states, respectively. The region of interest in this study is the absorption near

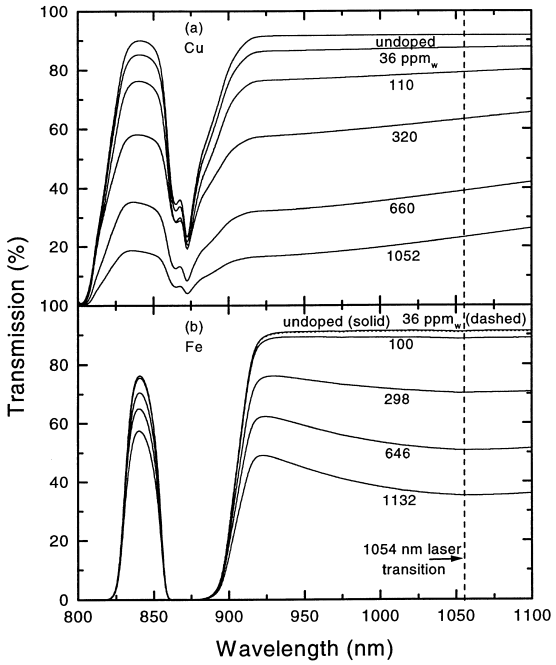

Fig. 1. Transmission spectra measured on LG-770 doped with various concentrations of (a) Cu and (b) Fe. The vertical dashed line represents the 1053 nm Nd^{3+} laser transition. The Cu and Fe spectra shown here are for nominal 0.5-cm and 5-cm-thick samples, respectively.

1053 nm that corresponds to the $^4F_{3/2}$–$^4I_{11/2}$ laser transition.

Fig. 2 shows the measured transmission spectra for LG-770 doped with various Fe impurity concentrations but without Nd^{3+}; La^{3+} was substituted as the rare-earth dopant. Because of the lack of interference by the Nd^{3+} absorption bands, these spectra show the major absorption bands due to Fe^{2+} and Fe^{3+} between about 300–3000 nm. The band assignments shown are based on reported values for Fe in phosphate glasses [14,17,39,40]. The absorption below 400 nm is due to the tail of the intense absorption bands of Fe^{3+} charge transfer states at about 195 and 240 nm [40,41]. Kurkjian and Sigety [17] assign the bands at about 415, 520 and 735 nm (Fig. 2(b)) to the Fe^{3+} transitions $^6A_1$–$^4E^4A_1$, $^4T_2$ and $^4T_1$, respectively.

The results from transmission measurements on the Cu, Fe and rare earth-doped samples are

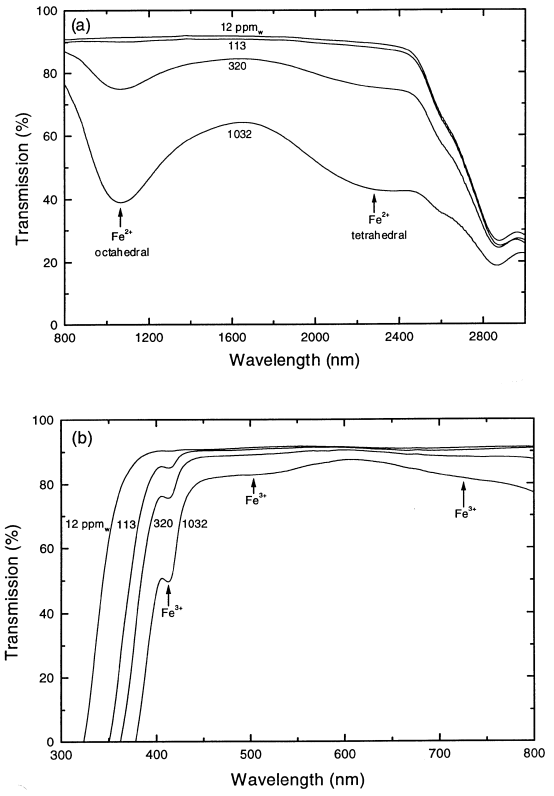

Fig. 2. Transmission spectra between (a) 800–3000 nm and (b) 300–800 nm for 5-cm-thick samples of LG-770 doped with various concentrations of Fe and using La rather than Nd as the rare-earth dopant.

summarized in Table 1 as extinction coefficients at 1053 nm. The extinction coefficients for the rare earths in LG-770 follow the observed trend: Dy $\gtrsim$ Sm $\gtrsim$ Pr > Ce. The extinction coefficients, ε (cm^{-1}/ppmw), were calculated from the measured absorption coefficients, α (cm^{-1}), by simply dividing by the impurity concentration (ppmw). It is straightforward to convert these reported extinction coefficients to other common concentration units (e.g. ions/cm^3, mol/l) from the known glass densities (2.83 and 2.59 g/cm^3 at 20°C for LHG-8 and LG-770, respectively).

3.2. Non-radiative decay rates

The increase in the Nd^{3+} fluorescence decay rate (i.e. quenching rate) due to the presence of the various metal ion impurities is summarized in Table 1 (Hz/ppmw). The quenching rate was computed from the measured fluorescence lifetimes

$$k_A = \frac{\left(\tau^{-1} - \tau_0^{-1}\right)}{[A]}, \tag{5}$$

where τ and τ_0 are the Nd^{3+} fluorescence lifetimes for the doped and undoped samples, respectively, $[A]$ is the impurity (acceptor) ion concentration, and k_A is the decay rate per unit impurity-ion concentration. The Nd concentration is fixed.

The quenching rate by Cu is nearly 10-fold greater than Fe at ion concentrations of more than

Table 1
Extinction coefficients at 1053 nm and fluorescence quenching rates due to various impurity ions in LG-770 and LHG-8 melted under oxidizing conditions (1 atmosphere O_2)[a]

Element	Quenching rate k_A (Hz/ppm)		Extinction coefficient ε (10^{-3} cm^{-1}/ppmw)	
	LHG-8	LG-770	LHG-8	LG-770
Cu	10.2 ± 1.5	10.6 ± 1.5	2.78 ± 0.34	2.61 ± 0.28
Fe ($\geqslant$ 1000 ppmw)	0.86 ± 0.03	1.4 ± 0.06	0.11 ± 0.005	0.18 ± 0.008
Fe (<1000 ppmw)	Eq. (9)[b]	Eq. (9)[b]	Eq. (6)[c]	Eq. (6)[c]
Dy	–	0.89 ± 0.04	–	0.016 ± 0.0006
Pr	1.1 ± 0.06	0.72 ± 0.04	–	0.012 ± 0.0005
Sm	–	0.63 ± 0.03	–	0.013 ± 0.0005
Ce	–	0.061 ± 0.03	–	0.0084 ± 0.0003

[a] The data are for Nd-doping densities of $4.6(\pm 0.1)$ and $4.2(\pm 0.1) \times 10^{20}$ ions/cm^3 for LG-770 and LHG-8, respectively.
[b] See Eq. (9): $\beta = 7.8$ kHz/cm^{-1} and ε_{Fe} per Eq. (6).
[c] See Eq. (6): $\varepsilon_{max} = 1.8(\pm 0.17) \times 10^{-4}$ cm^{-1}/ppm and $1.1\ (\pm 0.09) \times 10^{-4}$ cm^{-1}/ppm for LG-770 and LHG-8, respectively; $[Fe]_c = 170$ ppmw.

300 ppmw (i.e. about 10 Hz/ppmw Cu vs. 1 Hz/ppmw Fe). The Fe quenching rate is about 40% lower in LHG-8 compared to LG-770; however the Cu quenching rates are nearly identical in both glasses.

The effect of the rare earth impurities on the Nd^{3+} non-radiative decay rate in LG-770 varies from about 0.06–0.9 Hz/ppmw (Table 1) and follows the trend: $Dy \gtrsim Pr \approx Sm > Ce$. This trend approximately parallels that observed for the absorption cross-section of these ions (Table 1). LHG-8 samples doped with Pr^{3+} showed about a twofold greater decay rate than LG-770: 1.1 Hz/ppmw at 4.2×10^{20} Nd ion/cm^3.

4. Discussion

4.1. Optical absorption by Cu at 1053 nm

The Cu^{2+} absorption at 1054 nm increases linearly with Cu-doping concentration giving an extinction coefficient of about 2.7×10^{-3} cm^{-1}/ppmw in both LHG-8 and LG-770 (see Fig. 3). The magnitude of the Cu^{2+} extinction coefficient is similar to that observed in other phosphate laser glasses (Table 2). In particular, Sapak et al. [27] report a value of 2.7×10^{-3} cm^{-1}/ppmw measured for LG-750 prepared in an O_2 melting atmosphere. The composition of LG-750 is reported to be nearly identical to LHG-8 [4]. Here we assume Cu is present only as Cu^{2+} based on the work of Bae and Weinberg [13] who report 100% Cu^{2+} in fully equilibrated melts prepared in air using quartz crucibles and containing less than 50% CuO. All the melts in our study were prepared using quartz crucibles and O_2 and thus satisfy this criteria. Note that Sapak et al. [27] report that melts of LG-750 meta-phosphate containing Cu and prepared under neutral conditions (N_2) have extinction coefficients at 1053 nm about 20% lower than melts prepared in O_2 (Table 2). This suggests some conversion (~20%) of Cu^{2+} to Cu^{+} under these conditions.

Extinction coefficients for Cu impurities at ppmw concentrations in other glass forming systems have been reported. Ehrt [26] reports a value of about 7×10^{-4} cm^{-1}/ppmw in a fluorophosphate glass ($10Sr(PO_3)_2$–$35AlF_3$–$30CaF_2$–$15SrF_2$–$10MgF_2$) prepared using O_2 bubbling through the melt. Stokowski and Krashkevich [7] measured a value of 3.8×10^{-4} cm^{-1}/ppmw in a commercial alkali-zinc-silicate laser glass (LG-660) melted under neutral (N_2) conditions. These extinction coefficients are about 4–8 times lower, respectively, than observed in phosphate glasses.

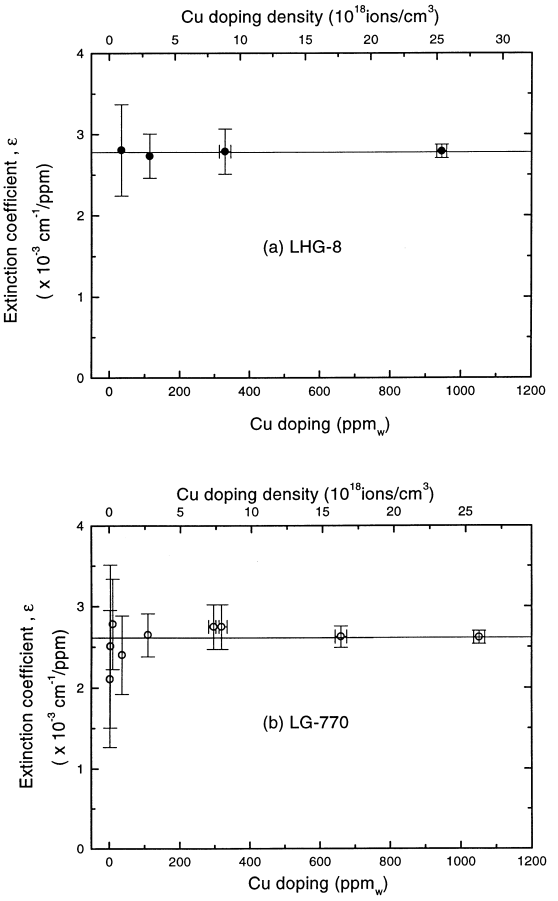

Fig. 3. Cu^{2+} extinction coefficient per ppmw at 1053 nm in LHG-8 (●) and LG-770 (○) as a function of Cu^{2+}-doping density.

4.2. Optical absorption by Fe

In contrast to Cu^{2+}, the extinction coefficient for Fe at 1053 nm is concentration dependent below about 300 ppmw (Fig. 4). We propose that this concentration dependence is due to a shift in the

Table 2
Comparison of extinction coefficients ($\times 10^{-3}$ cm^{-1}/ppmw) at 1053 nm from this study with previous work on phosphate laser glasses (doping concentrations greater than 300 ppmw)[a]

Source	This study		Toratani [28,29]	Stokowski and Krashkevich [7]		Sapak et al. [27]	
Glass	LG-770	LHG-8	GPP[b]	UP-91[b]	UP-16[b]	LG-750[b]	LG-750[b]
Atmosphere	O_2	O_2	–	N_2	N_2	O_2	N_2
Impurity							
Cu	2.6	2.8	2.4	2.3	2.1	2.7	2.1
Fe ($\geqslant$ 1000 ppmw)	0.18	0.11	2.4	0.7	0.6	0.13	0.55
Fe (<1000 ppmw)	Eq. (6)[c]	Eq. (6)[d]	–	–	–	–	–
Dy	0.016	–	0.011	–	–	–	–
Pr	0.012	$\leqslant$ 0.01	–	–	–	–	–
Sm	0.013	–	0.011	–	–	–	–
Ce	0.0084	–	–	–	–	–	–

[a] Random errors for values from this study are given in Table 1.
[b] GPP: 51.5 P_2O_5–18.5GeO_2–30GaO_2; UP-91 (ultraphosphate): 68.2 P_2O_5–11.8Al_2O_3–14K_2O–6$(La + Nd)_2O_3$; UP-16: 70 P_2O_5–20 K_2O–10 $(La + Nd)_2O_3$; LG-750[4] (meta-phosphate): (55–60) P_2O_5–(8–12)Al_2O_3–(13–17)K_2O–(10–15) BaO–(0–2)Nd_2O_3.
[c] LG-770: $\varepsilon_{max} = 0.179 \times 10^{-3}$ cm^{-1}/ppmw, $[Fe]_c = 170$ ppmw.
[d] LHG-8: $\varepsilon_{max} = 0.106 \times 10^{-3}$ cm^{-1}/ppmw, $[Fe]_c = 170$ ppmw.

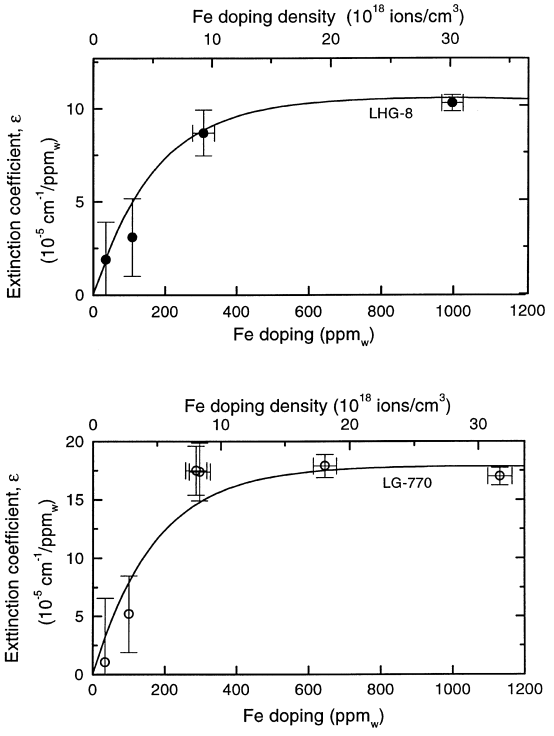

Fig. 4. Fe extinction coefficient at 1053 nm in LHG-8 (●) and LG-770 (○) as a function of Fe-doping density. The line is calculated using Eq. (6).

redox equilibrium between Fe^{3+} and Fe^{2+} at low doping levels. It is well known that Fe in glasses is distributed between Fe^{2+} and Fe^{3+} and that this distribution depends on the redox state of the glass. In a study of barium aluminophosphate glasses, Zirkelbach and Brückner [14] estimate the distribution to be about 23% Fe^{2+}/77% Fe^{3+} and 25% Fe^{2+}/75% Fe^{3+} for their glasses when melted in air and O_2, respectively. This distribution is for a Fe doping level of 1 mol%. They also determined the distribution of Fe^{2+} between octahedral and tetrahedral coordination by measuring the intensities of the characteristic bands for these two sites near 1050 and 2100 nm, respectively.

The Fe 1053-nm extinction coefficient reported here is also dependent on the glass type, although this effect is much smaller than the doping concentration dependence. In particular, the Fe extinction coefficients differ by about a factor of two between LHG-8 and LG-770 samples for Fe concentrations of 300 ppmw or greater. The compositions of LHG-8 and LG-770 differ mainly in the group II modifiers they contain: BaO and MgO, respectively. Thus it is possible these modifiers alter the oxygen fugacity sufficiently to change the Fe^{2+}/Fe^{3+} ratio; such effects are well-known in silicate glasses (see for example [15,42,43]. It is also possible that the slightly different melt tempera-

tures used to prepare our glasses cause this difference. Specifically the LHG-8 and LG-770 samples were melted and refined at 1200/1375°C and 1100/1250°C, respectively. Standard melt thermodynamics favor Fe^{2+} formation at higher temperatures [20,21,43,44] that could account for the higher Fe^{2+} in the LG-770 sample.

A comparison of the Fe extinction coefficients at 1053 nm determined from the optical transmission measurements and via laser calorimeter is given in Fig. 5. Absolute calibration of the calorimeter is difficult but relative changes in absorption can be readily measured. Therefore in Fig. 5 we compare the relative change in sample absorption measured via the calorimeter with that determined by direct transmission measurements on both LHG-8 and LG-770 samples. Data from these two measurement techniques agree to within the error limits shown (Fig. 5).

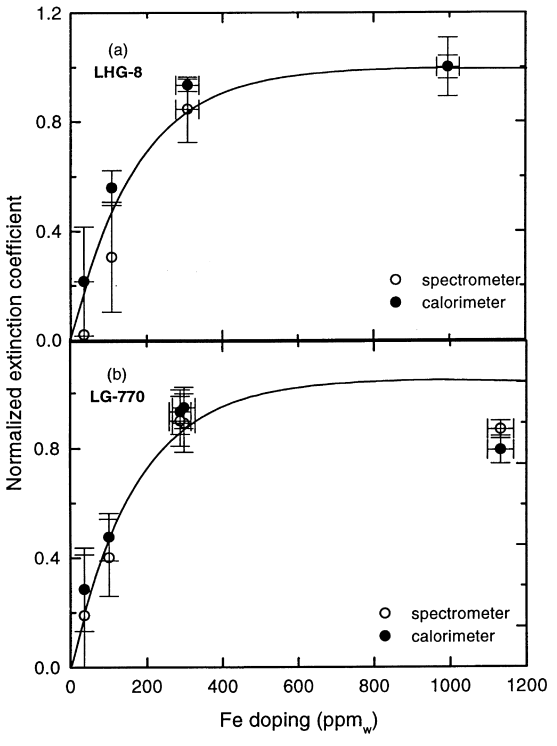

Fig. 5. Normalized extinction coefficient at 1053 nm as a function of varying Fe-doping concentrations as measured by spectroscopic and calorimetric methods for LHG-8 and LG-770. The solid line is Eq. (6) with ε_{max} normalized to 1.

To more fully analyze our data, we chose to fit the measured Fe extinction coefficient at 1054 nm to a single parameter equation of the form

$$\varepsilon_{Fe} = \varepsilon_{max}(1 - \exp(-[Fe]/[Fe]_c)), \quad (6)$$

where, ε_{Fe}, is the Fe extinction coefficient, ε_{max}, the limiting extinction coefficient at Fe concentrations of 1000 ppmw and [Fe], the Fe doping concentration (ppmw). The parameter, $[Fe]_c$, is a characteristic doping density for the system and is the single fitting parameter. The best fit to the data for both LG-770 and LHG-8 samples gives $[Fe]_c = 170$ ppm. The measured ε_{max} are 1.79×10^{-4} and 1.06×10^{-4} cm^{-1}/ppm for LG-770 and LHG-8, respectively (see Fig. 4).

The data in Fig. 2 show there is little change with concentration in the Fe^{2+} distribution between sites of tetrahedral and octahedral coordination. Instead, the dominant reason for the drop in 1053 nm absorption appears to be due to the redistribution in Fe between the 2+ and 3+ states. The change in the ratio of Fe^{3+}/Fe^{2+} can be measured from the change in intensity ratios for bands associated with 3+ and 2+ ions.

The change in the Fe^{2+}/Fe^{3+} ratio at low dopings was verified not only by measuring the decrease in Fe^{2+} but also the corresponding increase in Fe^{3+} using the characteristic band at 415 nm. These data are plotted in Fig. 6 as normalized Fe^{2+} and Fe^{3+} extinction coefficients, for various Fe doping levels. The extinction coefficients are both constant above about 300 ppmw, however below 300 ppmw the extinction coefficient for the 415 nm bands (Fe^{3+}) increases whereas the value for the 1050 nm band (Fe^{2+}) decreases. The data in Fig. 6 are meant to illustrate the increase in Fe^{3+}; however, the absolute magnitude of the increase should be viewed with caution because of the lack of a numerical band fitting analysis.

The observed change of the Fe^{2+}/Fe^{3+} ratio without a corresponding change in melting conditions (i.e. the oxygen pressure over the melt) is unusual but not without precedence. Glebov et al. [45] has reported similar behavior for Fe in silicate glasses at low doping levels ($\leqslant 500$ ppmw Fe doping). Glebov suggests that at high Fe concentrations the Fe^{2+}/Fe^{3+} ratio is determined by the

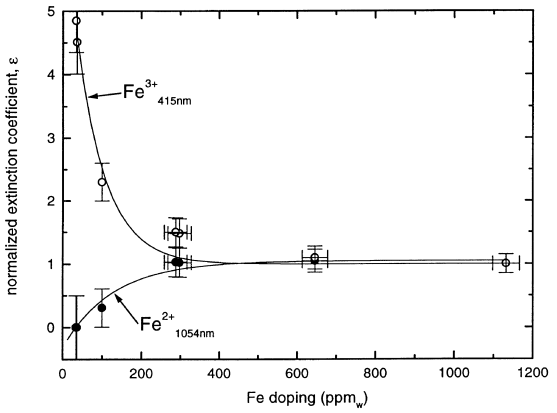

Fig. 6. Relative change in the Fe^{2+} (415 nm) and Fe^{3+} (1053 nm) extinction coefficients with change in Fe-doping density; values are normalized to the extinction coefficients at the high concentration limit (1100 ppmw).

structural association (i.e. correlation) between the Fe^{2+} and Fe^{3+} ions because of their close proximity. However, he proposes that at low concentration the ions become spatially separated and are no longer correlated and consequently, the Fe^{2+}/Fe^{3+} ratio changes due to localized site (structural) changes. If Glebov's physical description is correct, then the characteristic Fe–Fe interatomic distance for this change corresponds to the average spatial separation at the characteristic iron concentration (Fe_c) determined via Eq. (6). This separation is about 55 Å for $Fe_c \approx 170$ ppmw.

In a related study, Bae and Weinberg [13] report changes in the Cu^{2+}/Cu^{+} ratio with total Cu concentration even though the melt environment remains unchanged. Like Glebov, they also suggest this is due to structural (site accommodation) effects.

4.3. Optical absorption by Dy, Sm, Pr and Ce

The extinction coefficients reported here for Dy and Sm in LG-770 are similar to the values reported by Toratani [28] for a germanium–gallium phosphate glass (Table 2). Similarly the value for Pr is only about 10–30% lower than Sm and Dy, respectively. The extinction coefficient for Ce is about 50–100% lower than the other rare earths for these samples melted in 100% O_2. The small extinction coefficients are simply representative of the fact that only the tails of the characteristic absorption bands for these rare earths extend to 1053 nm [46].

4.4. Analysis of measured quenching rates

The measured quenching rates are analyzed using the Förster–Dexter theory for dipolar energy transfer [7,9,10] that was discussed in Section 1. The quantity k_{DA} given by Eq. (3) is equal to the measured quantity $k_A[A]$ from Eq. (5) and thus

$$k_A = \frac{\eta R_{DA}^{-6}}{[A]} \int \frac{K_A(v)\, G_D(v)\, dv}{v^4}. \tag{7}$$

The data in Fig. 1 show that the impurity absorption, $K_A(v)$, is approximately constant over the frequency region of the donor emission bands and thus, this term can be moved outside the integral

$$k_A = \frac{\eta R_{DA}^{-6} \overline{K}_A}{[A]} \int \frac{K_D(v)\, dv}{v^4}, \tag{8}$$

where $\overline{K}_A$ is the mean absorption over the emission band and is proportional to ε_A $[A]$, the acceptor extinction coefficient at the emission band maximum. Eq. (8) can now be written in the useful form

$$k_A = \beta \varepsilon_A, \tag{9}$$

where β is a constant for a fixed Nd concentration and a given glass composition

$$\beta = \eta'[D] \int \frac{K_D(v)\, dv}{v^4}. \tag{10}$$

Note that we have replaced ηR_{DA}^{-6} with $\eta'[A][D]$, where $[D]$ is the Nd (donor) concentration. The Nd concentration used in this study, $\sim 4 \times 10^{20}$ ions/cm^3 while the impurity doping densities are $< 0.3 \times 10^{20}$ ions/cm^3. In words, Eq. (9) states that the measured decay rate, on a per-ion basis, should vary directly with the impurity (acceptor) extinction coefficient for samples containing a fixed Nd doping level. In the case of Cu^{2+}, the extinction coefficient is nearly constant for all Cu^{2+} doping concentrations in both LHG-8 and LG-770 samples (Fig. 3). Similarly the Nd decay rate per unit

Cu doping density (i.e. Hz/ppmw) is also nearly constant (Fig. 7) as predicted by Eq. (9).

In contrast to Cu^{2+}, the Fe extinction coefficient depends on the concentration as shown in Fig. 4 and discussed in Section 4.2. Therefore, based on Eq. (9), one expects the decay rate, k_{Fe}, to vary with the concentration in the same fashion as ε_{Fe}; this is found to be the case (Fig. 8). The line shown in Fig. 8 is calculated by the expression

$$k_{Fe} = \beta \varepsilon_{Fe}, \tag{11}$$

where ε_{Fe} is the extinction coefficient at 1053 nm for Fe given by Eq. (6) and β is 7.8 kHz/cm^{-1} as determined from the measured k_{Fe} and ε_{Fe} at Fe doping concentrations of 1000 ppmw.

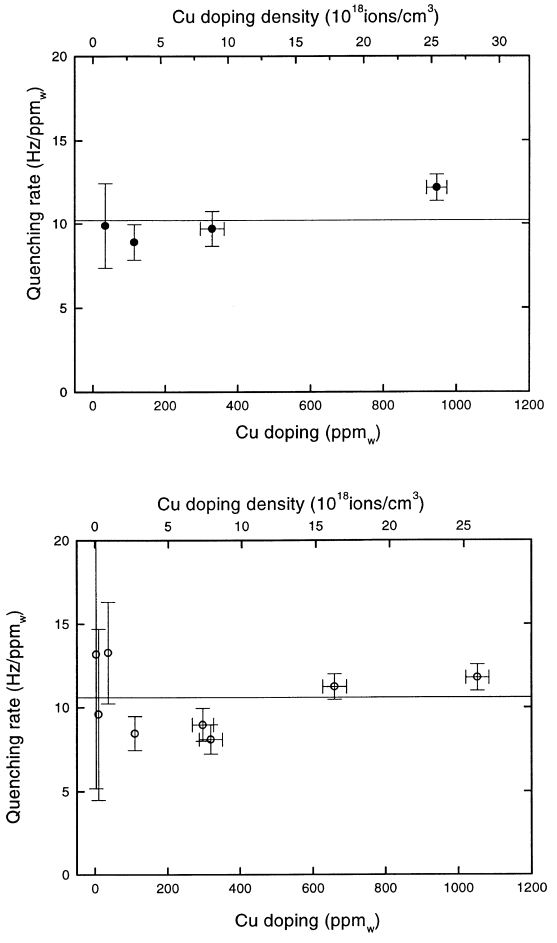

Fig. 7. Nd^{3+} fluorescence quenching rate as a function of Cu^{2+}-doping concentration for both LHG-8 (●) and LG-770 (○).

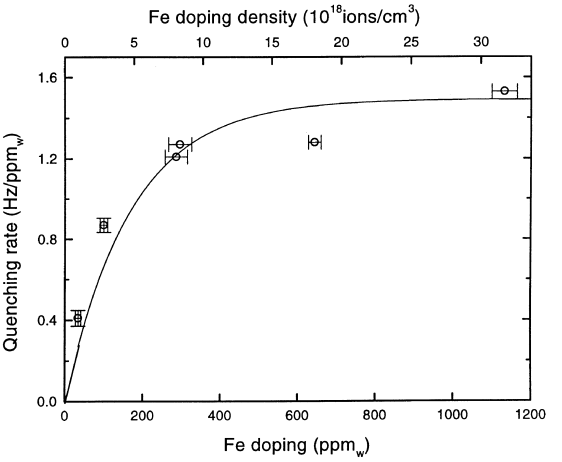

Fig. 8. Nd^{3+} fluorescence quenching rate for Fe in LG-770 as a function of Fe-doping density. The line is calculated using Eq. (11).

The quenching rate for the rare earths follows approximately the same trend as the extinction coefficients. Note however that whereas the extinction coefficients differ by more than 10–100 between the rare earths and Fe and Cu, respectively, the corresponding difference in quenching rates is about an order-of-magnitude less (Table 1).

5. Conclusions

The Fe extinction coefficient at 1054 nm in two meta-phosphate laser glasses decreases by more than 10-fold from about 1.1 and 1.8×10^{-4} cm^{-1}/ppmw to less than 1×10^{-5} cm^{-1}/ppmw with a change in Fe doping concentration from 1000 to 30 ppmw. In contrast, the extinction coefficient for Cu remains constant at about 2.7×10^{-3} cm^{-1}/ppmw over the same doping range. The quenching rates for these two ions follow the same behavior as the change in extinction coefficients as predicted by Förster–Dexter theory for dipolar energy transfer.

The unusual behavior of Fe is shown to be caused by a change in the Fe^{2+}/Fe^{3+} ratio even though the melt conditions remain constant. This change is proposed to be caused by structural effects on the redox distribution similar to that

reported by Glebov et al. [45] in silicates at low Fe doping concentrations.

The extinction coefficients at 1053 nm of the rare earths Dy, Sm, Pr and Ce are 10–100 times less than Fe and Cu at 1000 ppmw doping levels and follow the trend Dy $\gtrsim$ Sm $\approx$ Pr $>$ Ce. The quenching rates follow the same trend but are only about 2–10 times less than Fe and Cu, respectively.

Acknowledgements

The authors gratefully acknowledge the helpful discussions with Dr Leonid Glebov regarding the reason for the change in Fe^{2+}/Fe^{3+} ratio. The assistance by Ms B. Gober-Mangan, Mr J. Spaeth, and Ms T. Duewer on certain of the measurements presented in this work is appreciated. The assistance by Ms A. Clasen in the preparation of the manuscript is also deeply appreciated. Finally, the contributions by the late W.A. Steele on many aspects of the early stages of this study are deeply appreciated; he is fondly remembered and greatly missed. This work is supported by the US Department of Energy by Lawrence Livermore National Laboratory under contract W-7405-ENG-48.

References

[1] J.T. Hunt, D.R. Speck, Opt. Eng. 28 (1989) 461.
[2] B.M. Van Wonterghem, J.R. Murray, J.H. Campbell, D.R. Speck, C.E. Barker, I.C. Smith, D.F. Browning, W.C. Behrendt, Appl. Opt. 36 (1997) 4932.
[3] J. Murray, SPIE 3492 (1998) 1.
[4] J. Campbell, T. Suratwala, these Proceedings, p. 318.
[5] W. Koechner, Solid-State Laser Engineering, 4th Ed., Springer, New York, 1996.
[6] J. Campbell, T. Suratwala, C. Thorsness, J. Hayden, A. Thorne, J.M. Cimino, A. Marker, K. Takeuchi, M. Smolley, G. Ficini-Dorn, these Proceedings, p. 342.
[7] S.E. Stokowski, D. Krashkevich, Mater. Res. Soc. Symp. 61 (1986) 273.
[8] J.A. Caird, F.P. Milanovich, N.D. Nielsen, H.T. Powell, J.E. Marion, A.J. Pertica, J.N. Roe, in: Proceedings of the Conference on Lasers and Electro-Optics (CLEO), 1989, p. 1.
[9] T. Förster, Ann. Phys. 2 (1948) 56.
[10] D.L. Dexter, J. Chem. Phys. 21 (1953) 836.
[11] A.M. Bishay, L. Makar, J. Am. Ceram. Soc. 52 (1969) 605.
[12] B. Kumar, J. Am. Ceram. Soc. 74 (1991) 226.
[13] B.S. Bae, M.C. Weinberg, J. Am. Ceram. Soc. 74 (1991) 3039.
[14] K. Zirkelbach, R. Brückner, Glastech. Ber. Glass Sci. Technol. 60 (1987) 312.
[15] J.A. Duffy, Phys. Chem. Glasses 40 (1999) 54.
[16] L.E. Bausa, J.G. Sole, A. Duran, J.M.F. Navarro, J. Non-Cryst. Solids 127 (1991) 267.
[17] C.R. Kurkjian, E.A. Sigety, Phys. Chem. Glasses 9 (1968) 73.
[18] G.K. Marasinghe, M. Karabulut, C.S. Ray, D.E. Day, M.G. Shumsky, W.B. Yelon, C.H. Booth, P.G. Allen, D.K. Shuh, J. Non-Cryst. Solids 222 (1997) 144.
[19] B. Pivac, A. Moguš-Milanković, D.E. Day, J. Non-Cryst. Solids 226 (1998) 41.
[20] D. Ehrt, M. Leister, A. Matthai, Molten Salt Forum 5&6 (1998) 547.
[21] A. Matthai, D. Ehrt, C. Russel, Glastech. Ber. Glass Sci. Technol. 71 (1998) 187.
[22] B. Kumar, C. Chen, Phys. Chem. Glasses 33 (1992) 204.
[23] L. Cook, K.H. Mader, J. Am. Ceram. Soc. 65 (1982) 597.
[24] D. Ehrt, W. Seeber, J. Non-Cryst. Solids 129 (1991) 19.
[25] D. Ehrt, M. Carl, T. Kittel, M. Müller, W. Seeber, J. Non-Cryst. Solids 177 (1994) 405.
[26] D. Ehrt, J. Non-Cryst. Solids 196 (1996) 304.
[27] D. Sapak, J. Ward, J. Marion, SPIE 970 (1988) 107.
[28] H. Toratani, PhD thesis, Kyoto University, Kyoto, 1989.
[29] H. Toratani, H.E. Meissner, T. Izumitani, S.E. Stokowski, J. Non-Cryst. Solids 95&96 (1987) 701.
[30] J.H. Campbell, E.P. Wallerstein, J.S. Hayden, D.L. Sapak, D.E. Warrington, A.J. Marker, Glastech. Ber. Glass Sci. Technol. 68 (1995) 11.
[31] J.H. Campbell, E.P. Wallerstein, H. Toratani, H.E. Meissner, S. Nakajima, T.S. Izumitani, Glastech. Ber. Glass Sci. Technol. 28 (1995) 59.
[32] T.I. Suratwala, R.A. Steele, G.D. Wilke, J.H. Campbell, K. Takeuchi, these Proceedings, p. 213.
[33] J.S. Hayden, A.J. Marker, T. Suratwala, J.H. Campbell, these Proceedings, p. 228.
[34] H. Ebendorff-Heidepriem, D. Ehrt, Glastech. Ber. Glass Sci. Technol. 68 (1995) 139.
[35] J. Shelby, ASM International, Materials Park, OH, 1996.
[36] S. Payne, M.L. Elder, J.H. Campbell, G.D. Wilke, M.J. Weber, in: A.J. Bruce, B.V. Hiremath (Eds.), Solid-State Optical Materials, American Ceramic Society, Westerville, OH 28, 1991, p. 253.
[37] A. Ramponi, J. Caird, J. Appl. Phys. 63 (1988) 5476.
[38] G.M. Barrow, Physical Chemistry, McGraw-Hill, New York, 1973.
[39] B. Camara, Glastech. Ber. Glass Sci. Technol. 51 (1978) 87.
[40] U. Kolberg, in: H. Bach, N. Neuroth (Eds.), The Properties of Optical Glass, ch. 8.8, Springer, Berlin, 1995, p. 351.
[41] W. Seeber, D. Ehrt, Glastech. Ber. Glass Sci. 70 (1997) 312.
[42] C. Rüssel, S. Gerlach, The Influence of Glass Composition on the Thermodynamics of the Fe^{2+}/Fe^{3+} Equilibrium, Fifth ESG Conference, Prague (1999), A1-18-A1-27.
[43] A. Paul, J. Non-Cryst. Solids 123 (1990) 354.

[44] A. Matthai, O. ClauBen, D. Ehrt, C. Rüssel, Glastech. Ber. Glass. Sci. Technol. 71 (1998) 29.
[45] L.B. Glebov, V.G. Dokuchaev, G.T. Petrovskii, M.N. Tolstoi, Sov. J. Glass Phys. 10 (1984) 90, English translation, Lawrence Livermore Laboratory, Report UCRL-UR-136672 (1999) 1–9.
[46] R.C. Powell, Physics of Solid-State Laser Materials, Springer, New York, 1998.